# UC Davis
## UC Davis Previously Published Works

**Title**

Common Structural Pattern for Flecainide Binding in Atrial-Selective Kv1.5 and Nav1.5 Channels: A Computational Approach

**Permalink**

**Journal**

**ISSN**

**Authors**

Mazola, Yuliet
Montesinos, José CE Márquez
Ramírez, David
et al.

**Publication Date**

**DOI**

**Copyright Information**

Peer reviewed

*Article*

# Common Structural Pattern for Flecainide Binding in Atrial-Selective $K_v1.5$ and $Na_v1.5$ Channels: A Computational Approach

Yuliet Mazola [1,†], José C. E. Márquez Montesinos [1,†], David Ramírez [2], Leandro Zúñiga [3], Niels Decher [4], Ursula Ravens [5], Vladimir Yarov-Yarovoy [6] and Wendy González [1,7,*]

1   Center for Bioinformatics, Simulation and Modeling (CBSM), Universidad de Talca, Talca 3460000, Chile; yuliet.mazola@utalca.cl (Y.M.); jose.marquez@utalca.cl (J.C.E.M.M.)
2   Departamento de Farmacología, Facultad de Ciencias Biológicas, Universidad de Concepción, Concepción 4030000, Chile; dramirezs@udec.cl
3   Escuela de Medicina, Centro de Investigaciones Médicas, Universidad de Talca, Talca 3460000, Chile; lzuniga@utalca.cl
4   Institute for Physiology and Pathophysiology, Vegetative Physiology, Philipps-University of Marburg, 35043 Marburg, Germany; decher@staff.uni-marburg.de
5   Institut für Experimentelle Kardiovaskuläre Medizin, Universitäts-Herzzentrum Freiburg Bad Krotzingen, 79110 Freiburg im Breisgau, Germany; ursula.ravens@uniklinik-freiburg.de
6   Department of Physiology and Membrane Biology, University of California, Davis, CA 95616, USA; yarovoy@ucdavis.edu
7   Millennium Nucleus of Ion Channels-Associated Diseases (MiNICAD), Talca 3530000, Chile
*   Correspondence: wgonzalez@utalca.cl
†   These authors contributed equally to this work.

**Abstract:** Atrial fibrillation (AF) is the most common cardiac arrhythmia. Its treatment includes antiarrhythmic drugs (AADs) to modulate the function of cardiac ion channels. However, AADs have been limited by proarrhythmic effects, non-cardiovascular toxicities as well as often modest antiarrhythmic efficacy. Theoretical models showed that a combined blockade of $Na_v1.5$ (and its current, $I_{Na}$) and $K_v1.5$ (and its current, $I_{Kur}$) ion channels yield a synergistic anti-arrhythmic effect without alterations in ventricles. We focused on $K_v1.5$ and $Na_v1.5$ to search for structural similarities in their binding site (BS) for flecainide (a common blocker and widely prescribed AAD) as a first step for prospective rational multi-target directed ligand (MTDL) design strategies. We present a computational workflow for a flecainide BS comparison in a flecainide-$K_v1.5$ docking model and a solved structure of the flecainide-$Na_v1.5$ complex. The workflow includes docking, molecular dynamics, BS characterization and pattern matching. We identified a common structural pattern in flecainide BS for these channels. The latter belongs to the central cavity and consists of a hydrophobic patch and a polar region, involving residues from the S6 helix and P-loop. Since the rational MTDL design for AF is still incipient, our findings could advance multi-target atrial-selective strategies for AF treatment.

**Keywords:** atrial fibrillation; multi-target; drug promiscuity; druggable binding site; flecainide; $Na_v1.5$; $K_v1.5$; binding site comparison; polypharmacology

## 1. Introduction

Atrial fibrillation (AF) is the most common arrhythmia worldwide [1]. Its management involves drugs to modulate ion channels' activity in cardiac cells. Most antiarrhythmic drugs (AADs) present nowadays in clinical practice possess a strong propensity for inducing ventricular arrhythmias coupled with systemic toxicity when used for long periods [2]. Additional efforts to develop novel drugs are needed [3].

Ideally, drugs against AF are expected to be selective for atrial over other cardiac functions in order to avoid ventricular proarrhythmia [4]. This selectivity is achieved by

targeting ion channels mainly expressed in atria or whose biophysical properties differ in atria versus ventricles tissues [4–6]. Well-known atrial-selective targets include $K_v1.5$, $Na_v1.5$ and the constitutively active Kir3.1/3.4 channels. They confer atrial selectivity by different mechanisms [4,7]. The $Na_v1.5$ channel (and its current, $I_{Na}$) is present in both atria and ventricle, but its biophysical properties are different in the atria, which confer atrial-selectivity to sodium channel blockers [4,7]. On the other side, $K_v1.5$ is preferentially expressed in atria over ventricles and therefore has been one of the main targets for atria-selective drug design purposes [8]. This channel carries $I_{Kur}$, the ultra-rapid delayed rectifier potassium current in atria but does not contribute to repolarizing currents in ventricles. When tested in humans, the $I_{Kur}$ block did not exhibit ventricular proarrhythmic activity. However, its efficacy in suppressing AF has been disappointing [9,10].

In contrast to the selective $I_{Kur}$ blockade, multi-channel blockers have progressed further in the clinic [11]. For example, amiodarone is one of the most effective antiarrhythmic drugs. Its action depends on a multi-target effect [2]. The advantages of a multi-channel blockade for AF are exemplified not only with a single-molecule blocker such as amiodarone but also with drug combinations [12,13]. Indeed, the need to explore drug combinations as an alternative for treating or preventing AF is gaining increasing relevance [3]. Several theoretical models were developed to study the effects of various drugs and their blockade of more than one ionic current in the setting of cardiac arrhythmia [14–16]. In detail, the combined $I_{Na}$ blockade with concomitant inhibition of rapid or ultrarapid delayed-rectifier $K^+$ currents ($I_{Kr}$ and $I_{Kur}$, respectively) enhanced anti-arrhythmic effects compared with the $I_{Na}$ blocker alone [14]. Importantly, although synergistic anti-arrhythmic effects emerge from combining the $I_{Na}$ blocker with $I_{Kur}$ and the $I_{Kr}$ blockade, only a combination with the atrial-selective $I_{Kur}$ block has no effect on ventricles [14]. In support of the relevance of the $I_{Na} + I_{Kur}$ blockade, Ni et al. [15] proposed with mathematical models that simultaneous blockage of these two currents produces synergism in electrically remodeled atria (which is a condition of chronic AF) without alterations in ventricles. It seems that multi-target directed ligands (MTDL) with a high degree of atrial-selectivity likely represent a favorable alternative to gain effective and safe antiarrhythmic drugs for treating AF.

In view of the above, we focused on $K_v1.5$ and $Na_v1.5$ given their potential as targets for MTDL design. Proteins that bind similar ligands usually have a similar structure or even share a similar binding site (BS) [17]. The $K_v1.5$ and $Na_v1.5$ channels belong to the voltage-dependent ion channel family and share a similar architecture and functional domains, including the voltage sensor domain and the ion-conducting pore domain (PD). In $Na_v1.5$, a single chain is arranged into four different repeats or domains (DI-DIV) adopting a pseudo-tetrameric fold. Similarly, four domains are also present in $K_v1.5$, but they are divided in four identical chains or subunits. To our knowledge, the comparison of the drug BS in ion channels is still limited; the first evidence of a common structural pattern in the $Na_v1.5$ and TASK-1 drug BS was recently reported [18]. The comparison of the BS contributes to an understanding of the promiscuity nature of a ligand, the discovery of new MTDLs, drug repurposing and analysis of side effects [19].

In the present work, we compared the $K_v1.5$ and $Na_v1.5$ respective BS for their common blocker flecainide from an in silico perspective. Flecainide was chosen because the availability of structural and mutagenesis data about its BS in $Na_v1.5$ and $K_v1.5$, respectively [20,21]. In addition, flecainide is frequently used for the management of AF [22–24]. Flecainide primarily blocks the fast $I_{Na}$ current from the $Na_v1.5$ channel and potassium channels including hERG (and its current, $I_{Kr}$) [25,26] and, to a lesser extent, $K_v1.5$ (and its current, $I_{Kur}$) [27,28]. For $K_v1.5$, flecainide blocks the $I_{Kur}$ current with a $IC_{50}$ of $38.14 \pm 1.06$ μM [21]. In the case of $Na_v1.5$, flecainide inhibition takes place with a low affinity ($IC_{50}$ = 345 μM). However, the affinity dramatically increases ($IC_{50}$ = 7.4 μM) when increasing the stimulation frequency as expected for use-dependent binding [29]. The flecainide blockade of hERG yielded a $IC_{50}$ of 1.49 μM [25]. This inhibitory effect, on $I_{Kr}$ and $I_{Na}$, occurs at lower concentrations, and it is likely the predominant effect during clinical use [25].

Here, we presented a computational workflow that allowed the flecainide BS comparison in $K_v1.5$ and $Na_v1.5$ based on the available rat $Na_v1.5$ ($rNa_v1.5$)-flecainide cryogenic electron microscopy (cryo-EM) structure and human $K_v1.5$ ($hK_v1.5$) functional studies for this drug [20,21]. This is the first effort to find a common structural pattern for flecainide binding in ion channels. We are beginning to gain a better understanding of how flecainide exerts its multi-target directed behavior in these atrial-selective ion channels.

## 2. Materials and Methods

### 2.1. Modeling Flecainide-$K_v1.5$ Complex

We performed an ensemble docking pipeline to obtain the flecainide-$K_v1.5$ complex (Scheme 1). We started by building the structural ensembles using 300 frames from the last 30 ns of one apo $K_v1.5$ molecular dynamics (MD) simulations (for one of the three replicas, the details of MD simulations are described below). The grid box ($25 \times 25 \times 25$ $Å^3$) was set including residues Thr-479, Ile-502, Val-505 and Ile-508 which are likely involved in flecainide binding, as reported in mutagenesis studies [21]. Flecainide is protonated in the piperidine ring at a physiological pH (pKa 9.3, 99% charged at pH 7.4). Protonated R-flecainide was prepared with LigPrep; the ligand parameters and charges were added according to the OPLS2005 force field [30–32]. Flecainide was docked to each frame using Glide software [33]. The docked poses were scored using the XP (extra precision) scoring function [34]. For each frame, the 10 best scored poses were saved. The average linkage method implemented in the Maestro suite [35] was used to cluster the flecainide docked poses. The complex with the lowest XP docking score (−5.866 kcal/mol) from the most populated cluster was selected as the reference model for the flecainide-$K_v1.5$ complex.
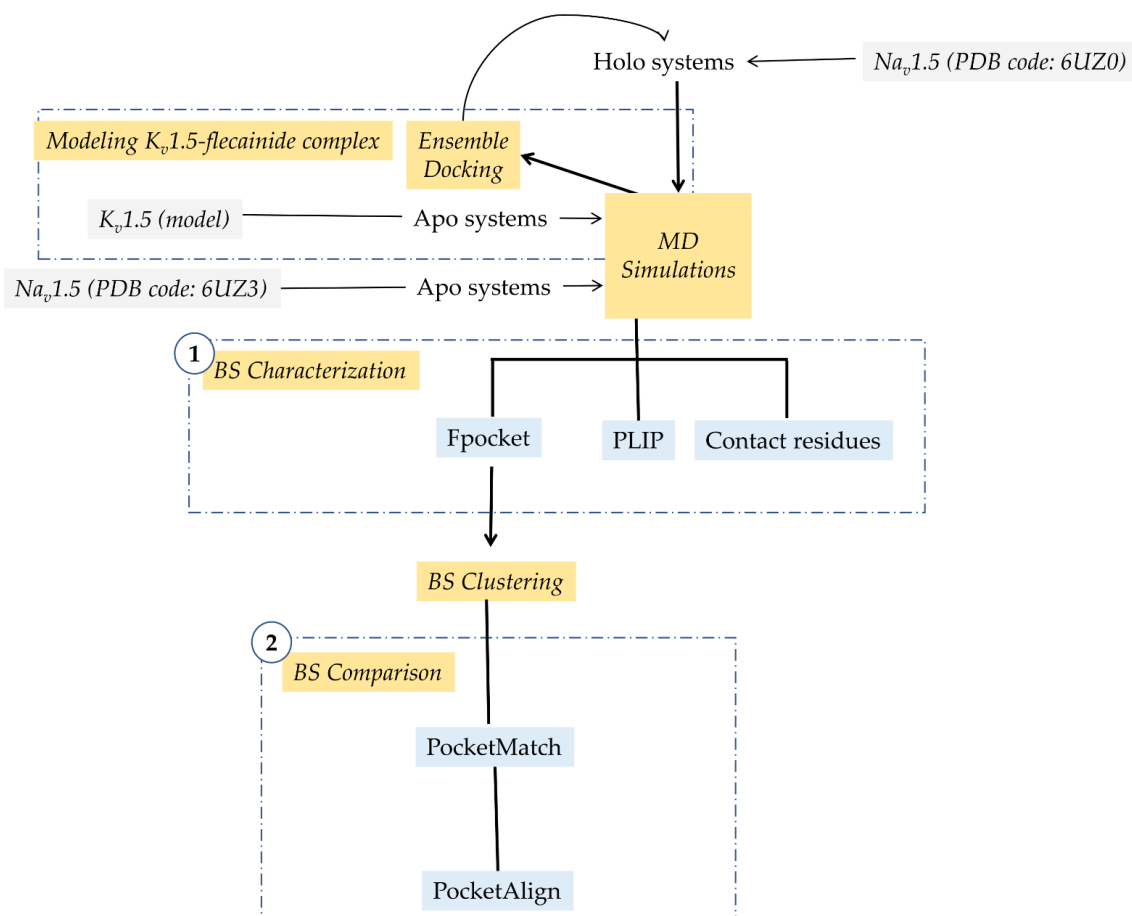


**Scheme 1. General workflow describing steps in methodology**. In color blue, software are displayed. The processes are indicated in yellow. *PDB: Protein Data Bank, BS: binding site, MD: molecular dynamics.*

## 2.2. Setting up Ion Channel Systems

Three 100 ns MD simulations for each system (apo/holo $K_v1.5$ and apo/holo $Na_v1.5$) were executed using the Desmond v2019-1 [36] and OPLS2005 force field [30–32]. Initial structures for holo MDs correspond to the flecainide-$K_v1.5$ model obtained herein and the cryo-EM structure of the r$Na_v1.5$-flecainide complex (PDB code: 6UZ0) [20]. Apo MDs were computed using, as input, the $K_v1.5$ homology-based model [37] and cryo-EM structure of r$Na_v1.5$ in its apo form (PDB code: 6UZ3) [20]. Target structures were prepared before MD simulations, completing side chains, checking protonation states and minimizing the potential energy of the structures using the Protein Preparation Wizard from the Maestro suite [35]. Systems were embedded into a pre-equilibrated POPC (1-palmitoyl-2-oleoyl-sn-glycero-3-phosphocholine) bilayer membrane model and solvated using the SPC (single point charge) water model. $Na^+/Cl^-$ ions for $Na_v1.5$ and $K^+/Cl^-$ ions for $K_v1.5$ were added to neutralize the systems, and then, NaCl or KCl was added to reach a concentration of 0.15 M in each case. $K^+$ ions were placed at sites S2 and S4 of the selectivity filter (SF) and water molecules at sites S1 and S3 in $K_v1.5$. No ions were located in the $Na_v1.5$ SF. Systems were equilibrated by 20 ns in the NPT ensemble. Positional restraints of 1.0 kcal $\times$ mol$^{-1}$ $\times$ Å$^{-2}$ were applied to all protein and ligand atoms in the $K_v1.5$ and $Na_v1.5$ systems. At the same time, the same positional restraints were applied to the ions and water molecules placed in the SF of the $K_v1.5$ channel. Temperature and pressure were kept constant at 300 K and 1.01325 bar, respectively, by coupling to a Nose-Hoover Chain thermostat [38] and Martyna-Tobias-Klein barostat [39]. The force field equation was integrated each at 2 fs in the MD simulations. Subsequently, positional restraints were removed, and 100 ns MDs were performed per system using a NP$\gamma$T (semi-isotropic ensemble) with the constant surface tension of 0.0 bar Å. Hence, there are 300 ns of MD production for apo and holo systems from three replicas for each channel. To check MDs' stabilization, root-mean-square deviation (RMSD) values of the proteins atoms were computed using TCL scripting in VMD v1.9.4a38 [40]. In total, 1.2 μs of the MD simulation were performed and analyzed. Structural and pore shaping changes were computed by root-mean-square-fluctuation (RMSF) of all atom residues in TCL scripting in VMD v1.9.4a38 [40] and HOLE software [41], respectively.

## 2.3. Flecainide Binding Site Characterization

For BS characterization purposes (Scheme 1, step 1), 1000 frames of each MD were retrieved, and the residues within 5 Å of flecainide were presumed to belong to the BS, a definition that will be kept in all the manuscript. For each frame, Fpocket [42] physicochemical features (area, volume, hydrophobicity proportion, Monera hydrophobicity score [43] and proportion of nonpolar atoms) were computed in the BS, calculating the mean and standard deviation in each point of the three replicas per system. Moreover, in the BS, contacting residues were counted using TCL scripting in VMD v1.9.4a38 [40]. The flecainide interaction profile was obtained using PLIP [44,45].

## 2.4. Flecainide Binding Site Comparison

All MDs of the holo systems were concatenated and underwent a clustering analysis (Scheme 1, step 2). This clustering was performed based on Fpocket physicochemical features computed in the previous section to retrieve representative structures for further analysis. The K-means algorithm with a euclidean distance implemented in R v4.1.2 and the NbClust package [46] was used to perform clustering and establish the optimum number of clusters, respectively. Two clusters were obtained per system (holo $K_v1.5$ and holo $Na_v1.5$), and the frame corresponding to the structure nearest to the computed K-means centroid was defined as representative structure of the cluster. Then, the representative structures were retrieved to compare their similarities by PocketMatch [47] using the previously defined BS (Scheme 1, Step 2). The comparison between the representative structures of the four clusters of $K_v1.5$ and $Na_v1.5$ resulted in one pair of centroids with the best score.

Then, PocketAlign software [48] was used to find amino acid correspondence in the pair of centroids with the best PocketMatch score.

### 2.5. Statistical Tests

The normality assumption was not satisfied by our data. For that reason, nonparametric statistical analysis was performed using R v4.1.2.

### 3. Results

This study compared the BS for flecainide in $K_v1.5$ and $Na_v1.5$ channels. In both channels, the PD provides BSs for most AADs and local anesthetics including flecainide BS [20,41,49–54]. Structurally, PD is composed of the helical segments S5, S6 and the loop connecting them (called P-loop). The latter contains the SF. In $K_v1.5$, the SF sequence is TVGYG and provides a row of $K^+$ coordination sites (called S1 to S4, from the extracellular to intracellular side of the cell membrane) [55]. In $Na_v1.5$, the SF is asymmetric and composed of a ring of four residues DEKA (from Asp in DI to Ala in DIV) [20].

As a first step in our computational pipeline, tertiary structures of flecainide in the complex with $K_v1.5$ and $Na_v.15$ are needed. For $K_v1.5$, a homology model reported by Marzian et al. [37] was used. In addition, we obtained the $K_v1.5$-flecainide complex using an ensemble docking pipeline. We considered that flecainide exhibits a preferential action for $K_v1.5$ in its open state with a Hill coefficient of about 1 [56]. Then, a unique ligand-BS or multiple non-cooperative ligand-BSs are anticipated. According to previous mutagenesis studies, residues from S6 helices (Ile-502, Val-505 and Ile-508) and the SF base (Thr-479, near to S4 $K^+$) are involved in the action of flecainide [21,28]. This evidence allowed us to focus solely on the central cavity (also known as the inner cavity) to explore a single putative BS for flecainide.

For $Na_v1.5$, the cryo-EM structure of $rNa_v1.5$ in the complex with flecainide (PDB code: 6UZ3) and its apo form (PDB code: 6UZ0) was used [20]. The flecainide-rNav1.5 complex is assumed in an intermediate inactivated state [20]. This fulfills our requirements since flecainide stabilizes the channel inactivation state [57]. Although we are especially interested in human $Na_v1.5$ ($hNa_v1.5$), the latter shares about 94% of global sequence identity with its homolog in the rat. Then, the results obtained here can be extended to the $hNa_v1.5$ channel.

Multiple MDs (three replicas) for $K_v1.5$ and $Na_v1.5$ channels in their apo and holo systems were executed during 100 ns. RMSD values are lower for $K_v1.5$, but all trajectories are stabilized after about 50 ns (Figure S1). We also check for structural changes upon flecainide binding between apo and holo systems in $K_v1.5$ and $Na_v1.5$ by computing RMSF. These results are presented in Figure S2 and evidence a global structure similarity between the apo and holo forms in both $K_v1.5$ (Figure S2a) and $Na_v1.5$ (Figure S2b). Moreover, in the PD (where flecainide binds), a local structural similarity between the apo and holo forms in $K_v1.5$ (Figure S2a) and $Na_v1.5$ (Figure S2b) is shown. The pore dimensions were also computed and compared between apo and holo systems (Figure S3). No differences were detected in pore size upon flecainide binding in $K_v1.5$ (Figure S3a). In the case of $Na_v1.5$, the pore was slightly enlarged (Figure S3b).

### 3.1. Flecainide Binding Mode and Interactions in $K_v1.5$

In our predictions, flecainide occupies the $K_v1.5$ central cavity (Figure 1a). Its piperidine moiety faces the pore but its trifluoromethyl groups protrude into the interface between subunits B and C. Residues in contact with flecainide (distance $\leq 5$ Å and frequency $\geq 70\%$, Figure 1b) recorded along with MD simulations and those having interactions with this drug (number of interactions $\geq 20$) are indicated in Figure 2a,b, respectively. The list of contacting residues includes Met-478.A, Thr-479.A, Thr-480.A, Gly-504.A, Val-505.A, Ile-508.A, Ala-509.A, Leu-437.B, Met-478.B, Thr-479.B, Thr-480.B, Ala-501.B, Ile-502.B, Gly-504.B, Val-505.B, Ile-508.B, Ala-509.B, Val-512.B, Ala-501.C, Ile-502.C and Val-505.C (Figures 1b and 2a).
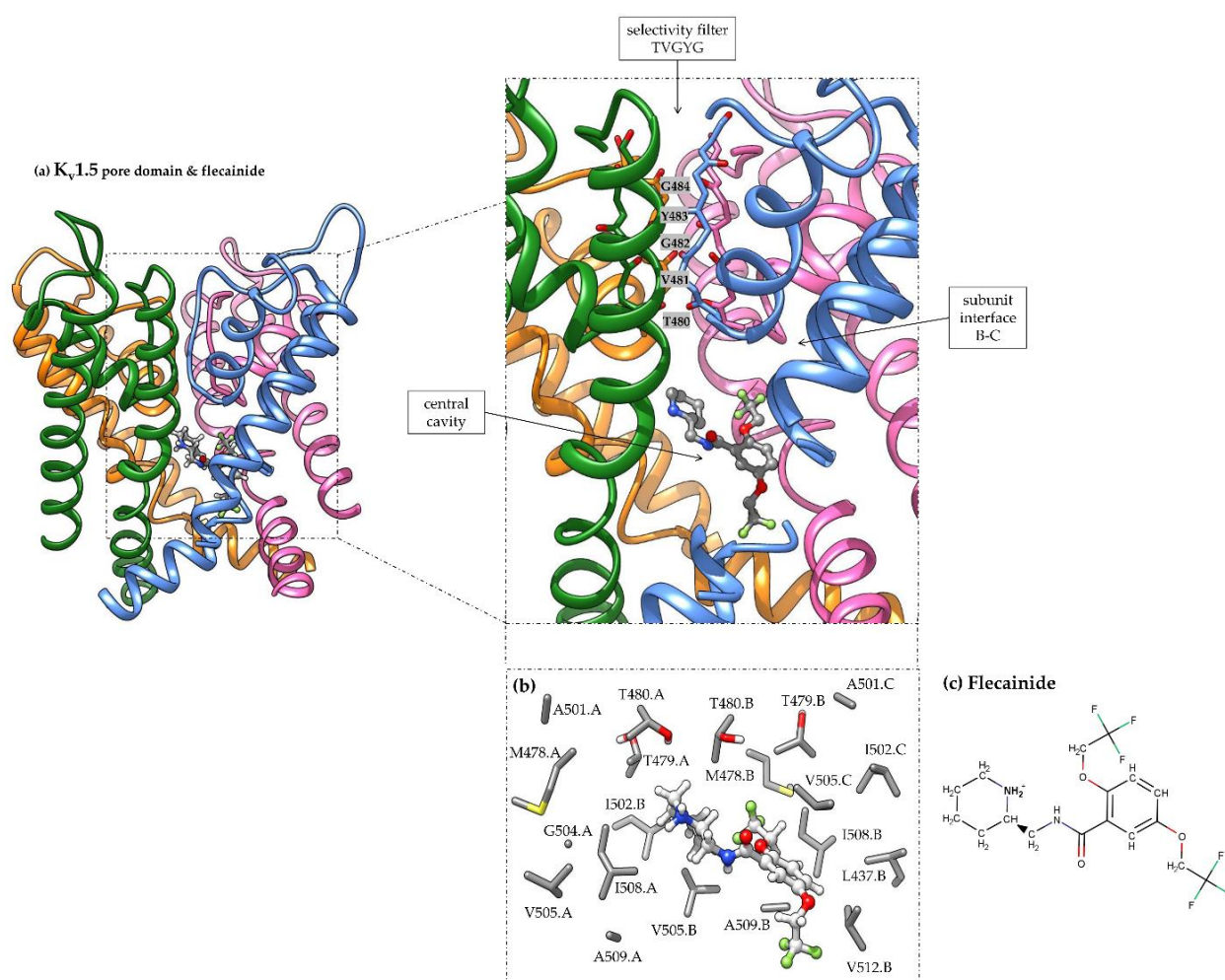
**Figure 1. Representation of flecainide binding mode in Kᵥ1.5 channel**. (**a**) Ribbon representation of Kᵥ1.5 pore domain; each subunit is shown in a different color: orange (subunit A), pink (subunit B), blue (subunit C), green (subunit D), and flecainide bound in the inner cavity is depicted in ball and sticks. Residues forming the selectivity filter are labeled and indicated in gray boxes. (**b**) Side-chain representation of residues in contact with flecainide (distance $\leq$ 5 Å) having a frequency of interaction $\geq$70% along MD simulations. Residue names and numbers are indicated. The tertiary structure used corresponds to a frame from the holo MD trajectories. (**c**) Flecainide representation in 2D format. Flecainide and residues are colored *per* element with carbon atoms in dark gray, oxygen atoms in red, nitrogen atoms in blue, sulfur atoms in yellow, hydrogens in light gray and fluorine in green.

The interactions involved are indicated in Figure 2b. Trifluoromethyl groups interact via the halogen-bond with residues Thr-479.A, Thr-479.B, Ala-501.C, Ile-502.C and Ile-508.B (Figures 1b and 2b). Hydrophobic interactions occurred with residues Thr-480.A, Thr-480.B, Val-505.A, Val-505.B, Ile-508.A, Ile-508.B, Ala-509.A and Ala-509.B (Figures 1b and 2b). Residues Thr-480.A, Thr-480.B and Thr-480.C interact with flecainide through water bridges. This residue is placed at the inner mouth of the SF. Residues Thr-479, Ile-502, Val-505 and Ile-508 were previously noticed as relevant for the flecainide effect in Kᵥ1.5 using mutagenesis studies [21,28].
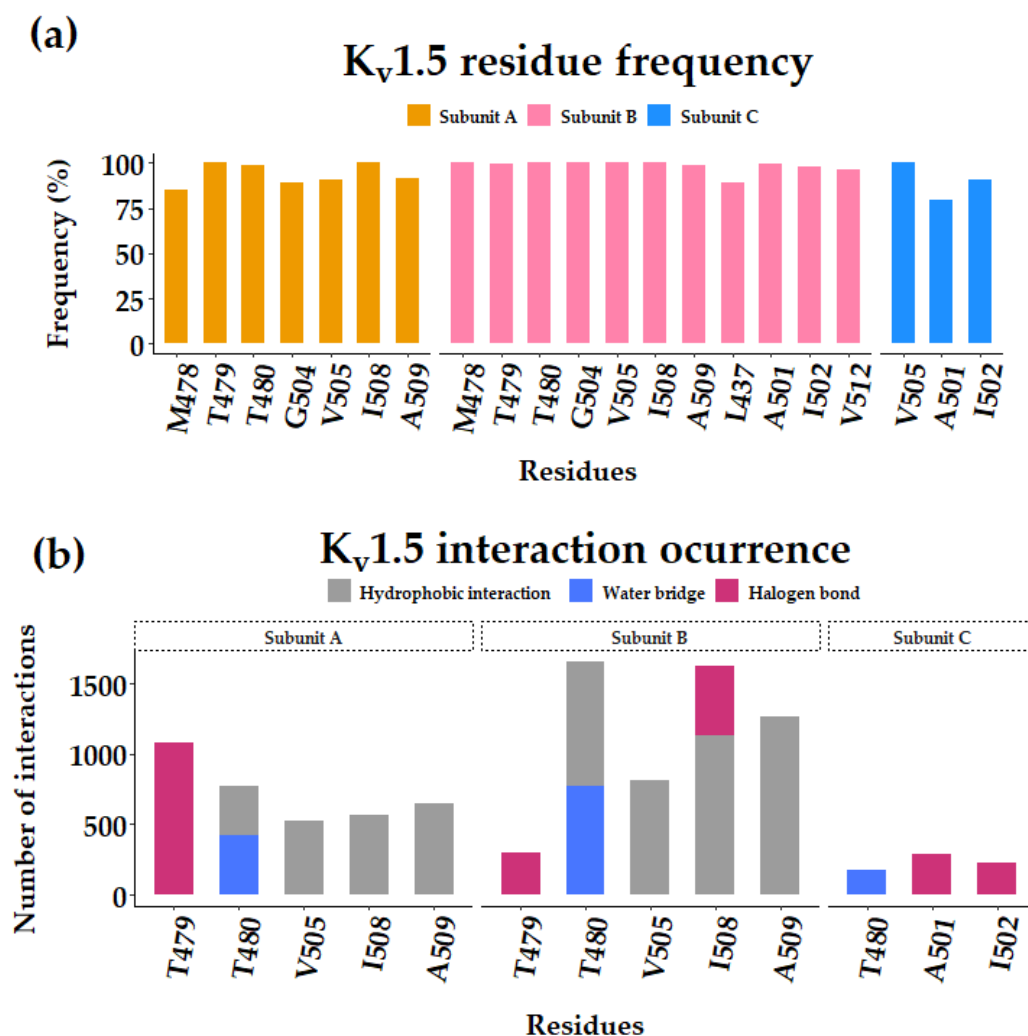
(a)

## $K_v1.5$ residue frequency



(b)

## $K_v1.5$ interaction ocurrence



**Figure 2. Flecainide interactions in $K_v1.5$ along MD simulations**. The residue contacts and interactions were computed along the three 100 ns MD simulations' replicas concatenated. (**a**) Residues in contact within 5Å of flecainide with a frequency of ≥70%. (**b**) Residues interacting with flecainide and the nature of such interactions predicted using PLIP software. Only the residues with number of interactions ≥20% of the maximum value of its type are considered.

*3.2. Flecainide Binding Mode and Interactions in $Na_v1.5$*

Similar to flecainide in $K_v1.5$, this drug is placed in the central cavity of $Na_v1.5$ below the SF (Figure 3a). In agreement with the cryo-EM flecainide-$Na_v1.5$ structure (PDB code: 6UZ3), our MDs' analysis confirms a number of residues that remain in close contact with flecainide: Leu-898.DII, Cys-899.DII, Val-933.DII, Phe-937.DII, Phe-1420.DIII, Ile-1456.DIII, Ile-1457.DIII, Phe-1461.DIII, Ile-1464.DIII and Phe-1762.DIV (Figures 3b and 4a). Other residues also found in close contact include Gln-372.DI, Val-406.DI, Asn-930.DII, Leu-934.DII, Thr-1419.DIII, Thr-1711.DIV, Ser-1712.DIV and Val-1765.DIV (Figure 4a).

For $Na_v1.5$ (Figures 3b and 4b), we noticed that hydrophobic interactions involve aromatic residues (e.g., Phe-937.DII, Phe-1420.DIII, Phe-1461.DIII and Phe-1762.DIV). Other residues also contribute to hydrophobic interactions, including Gln-372.DI, Val-933.DII, Leu-934.DII, Leu-1464.DIII and Val-1765.DIV. Trifluoromethyl moieties interact with residues Thr-371.DI, Leu-898.DII, Cys-899.DII, Asn-930.DII and Ile-1456.DIII. Water bridges connect the residues Thr-371.DI, Gln-372.DI, Cys-899.DII, Gly-900.DII, Asn-930.DII, Thr-1419.DIII, Phe-1420.DIII and Ser-1712.DIV with flecainide. In agreement with Jiang et al. [20], residues Leu-898.DII, Cys-899.DII, Val-933.DII, Phe-937.DII, Phe-1420.DIII, Ile-1456.DIII,

Ile-1457.DIII, Phe-1461.DIII, Ile-1464.DIII and Phe-1762.DIV remain in close contact with flecainide along MDs (Figures 3b and 4a).
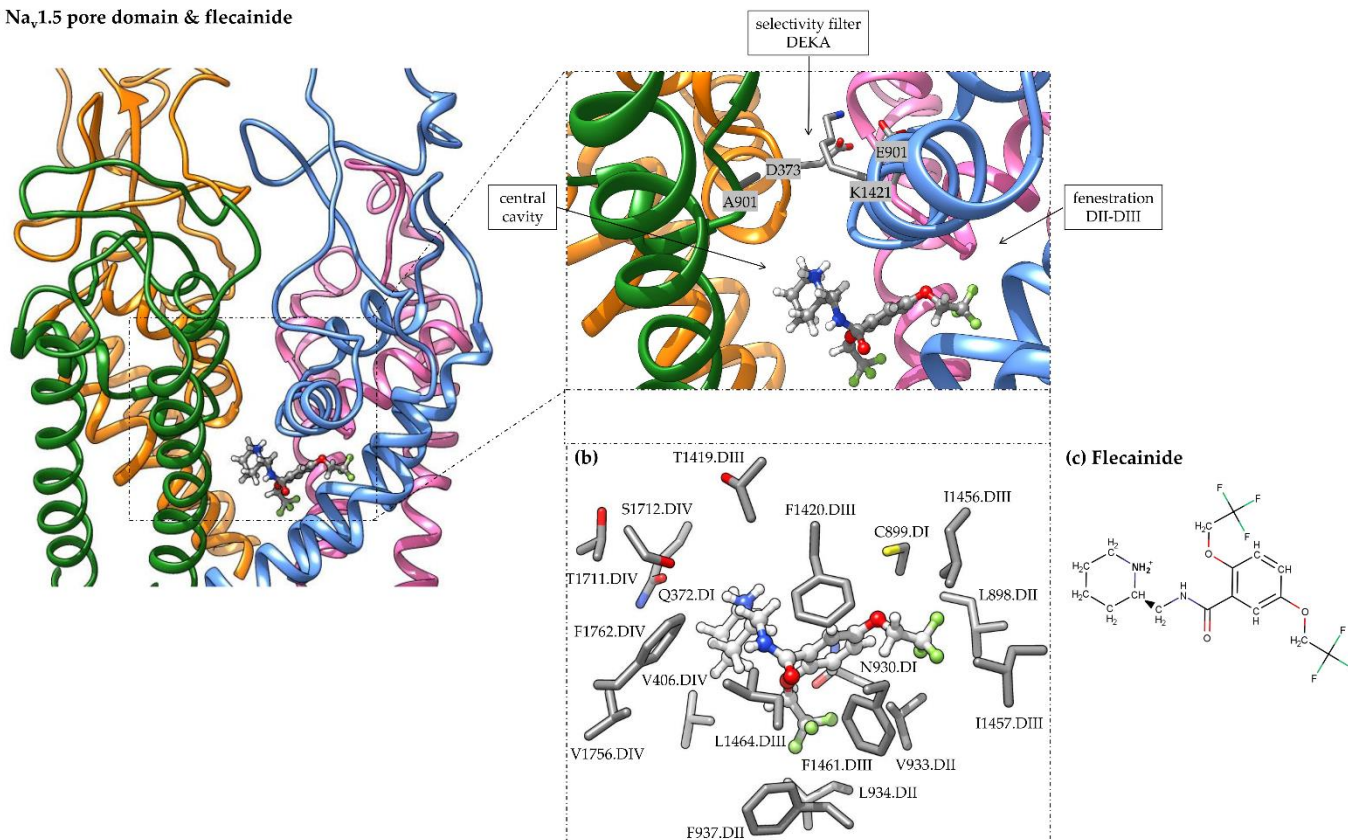


**Figure 3. Representation of flecainide binding mode in Na$_v$1.5 channel**. (**a**) Ribbon representation of Na$_v$1.5 pore domain; each domain is shown in a different color: orange (DI), pink (DII), blue (DIII) and green (DIV), and flecainide bound in the inner cavity is depicted in ball and sticks. Residues forming the selectivity filter are labeled and indicated in gray boxes. (**b**) Side-chain representation of residues in contact with flecainide (distance ≤ 5 Å) having a frequency of interaction ≥70% along MD simulations. Residue names and numbers are indicated. The tertiary structure used corresponds to a frame from the holo MD trajectories. (**c**) Flecainide representation in 2D format. Flecainide and residues are colored *per* element with carbon atoms in dark gray, oxygen atoms in red, nitrogen atoms in blue, sulfur atoms in yellow, hydrogens in light gray and fluorine in green.

Interestingly, we detected π-stacking interactions between the central phenyl group of flecainide and residues Phe-937.DII, Phe-1420.DIII and Phe-1461.DIII (Figures 3b and 4b). Most interactions occurred with Phe-1420.DIII.

### 3.3. Comparing Flecainide Binding Site

To compare flecainide pockets in K$_v$1.5 and Na$_v$1.5, we quantified physicochemical features using Fpocket in holo systems. We computed the volume (Figure 5a), area (Figure 5b), hydrophobicity proportion (Figure 5c), Monera hydrophobicity score (Figure 5d) and proportion of apolar atoms (Figure 5e) for each BS along MD simulations. Figure 5 shows that the flecainide pocket in K$_v$1.5 exhibits a higher volume and area. This assumption was ratified by the Wilconsox Rank Sum test (Figure 5). This is not surprising since voluminous phenylalanine aromatic residues shape the flecainide BS in Na$_v$1.5. When comparing the hydrophobic nature of both BSs, we found that both pockets are highly hydrophobic, Na$_v$1.5 being the one that presents the highest hydrophobicity according to the Wilconsox Rank Sum test in the measurements of hydrophobicity proportion, Monera hydrophobicity score [43] and proportion of apolar atoms (Figure 5c–e). Moreover, the residues accounting

for hydrophobicity differ in their side-chain size and volume between $K_v1.5$ and $Na_v1.5$ in the flecainide BS (Figures 1b and 3b).
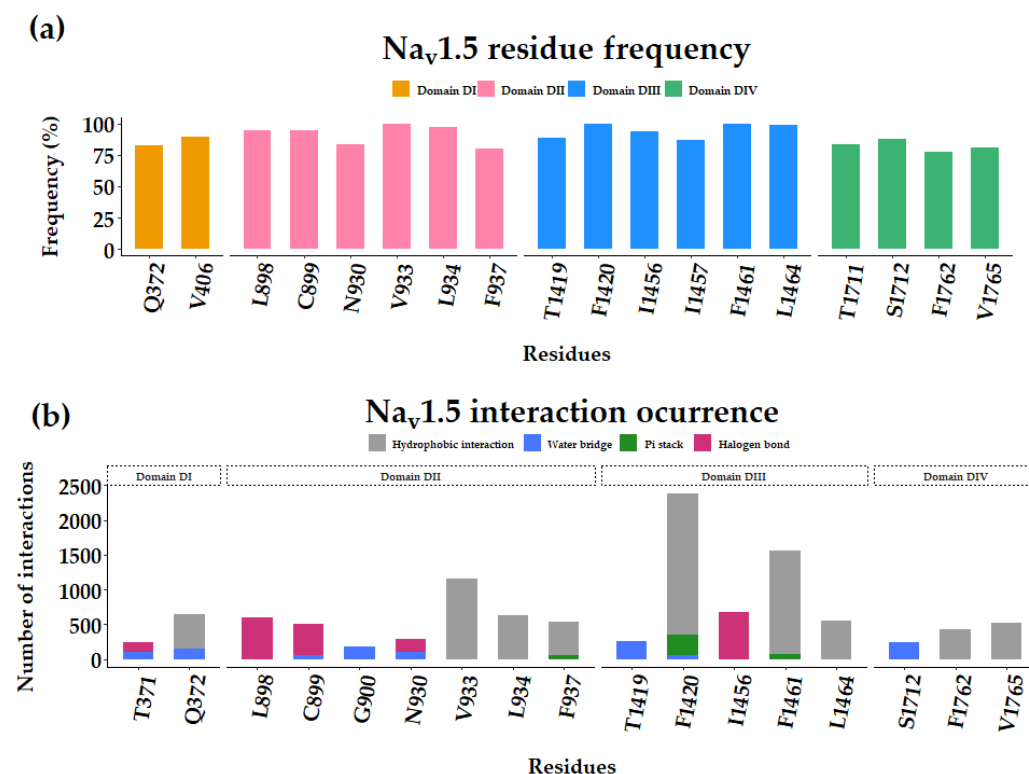
**(a)**



**(b)**



**Figure 4. Flecainide interactions in $Na_v1.5$ along MD simulations**. The residue contacts and interactions were computed along the 100 ns MD simulations. (**a**) Residues in contact within 5 Å of flecainide with a frequency of ≥70%. (**b**) Residues interacting with flecainide and the nature of such interactions were predicted using PLIP software. Only the residues with number of interactions ≥20% of the maximum value of its type are considered.

For a deep comparative analysis of the flecainide BS in the holo systems for $Na_v1.5$ and $K_v1.5$, we reduced the MD data by applying a clustering approach based on described physicochemical properties (Figure 5), as suggested by De Paris research [58]. The NbClust package performs a pre-running of K-means clusters calculation with different number of clusters, starting from 1. Then, NbClust computes 26 different indices. Each index determines an optimal number of clusters from previous K-means calculation. Finally, NbClust outputs the optimum number of clusters which is the most frequent value among the indices. In our case, we found that two clusters are the best choice for $K_v1.5$ and $Na_v1.5$ holo systems. For that reason, two centroids (representative frames) were retrieved from the 300 ns of each holo system. Regarding the flecainide-$K_v1.5$ complex, cluster 1 and cluster 2 consist of 1506 and 1494 structures from a total number of 3000 frames, respectively. The centroid for the first cluster corresponds to frame 979 from the first MD replica. The frame number 113 of the second MD replica was defined as the centroid of the second cluster. Both were renamed *$K_v1.5\_c1$* and *$K_v1.5\_c2$*, respectively. Likewise, on the flecainide-$Na_v1.5$ system, we obtained two clusters from a total number of 3000 frames where cluster 1 includes 1307 frames, and cluster 2 has 1693 frames. Frame number 43 from the third MD and number 458 from the first MD replica were computed as centroids and renamed, such as *$Na_v1.5\_c1$* and *$Na_v1.5\_c2$*, respectively. The BS residues from the centroids are described in Tables 1 and 2.

Centroids were compared using PocketMatch (Table 3). *$K_v1.5\_c2$* and *$Na_v1.5\_c2$* had the best PocketMatch similarity score between different channels (78.61%) in their flecainide

BS. This similarity score is similar to the one between BS from centroids of the same channel: *Na$_v$1.5_c1* and *Na$_v$1.5_c2* (83.27%).
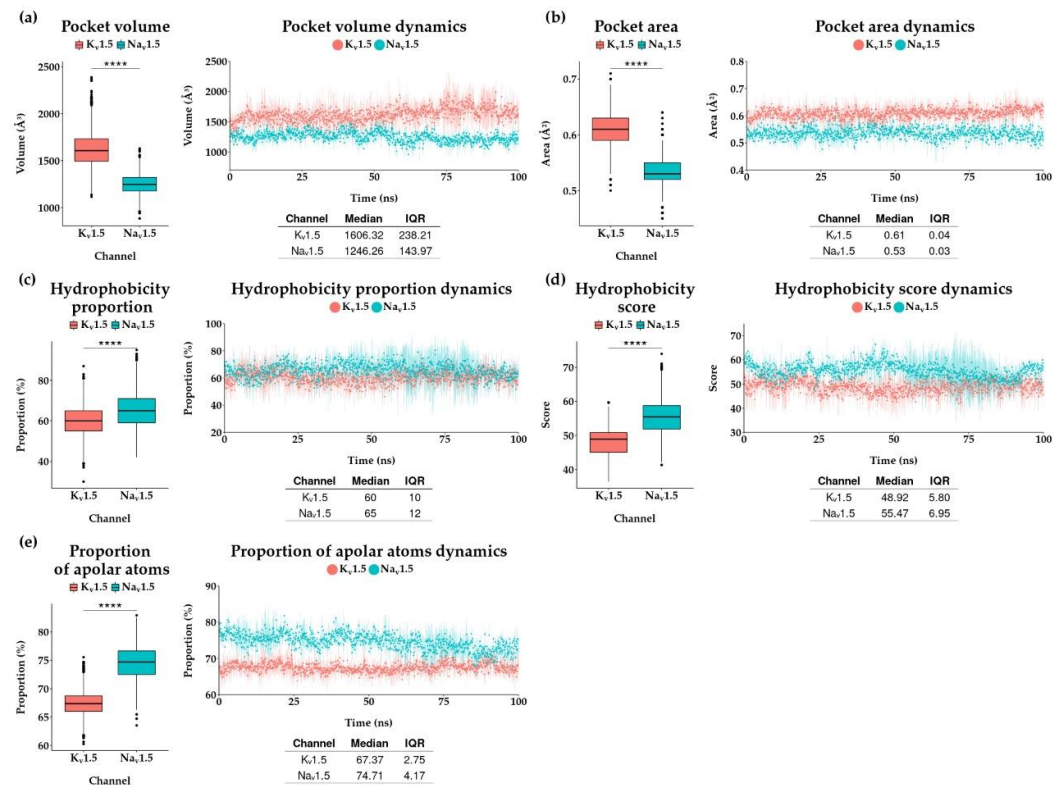


**Figure 5. Physicochemical characterization of flecainide binding site (BS)**. The flecainide BSs were computed in terms of (**a**) volume, (**b**) area, (**c**) hydrophobicity proportion, (**d**) Monera hydrophobicity score and (**e**) the proportion of apolar atoms in K$_v$1.5 and Na$_v$1.5 along three replicas of molecular dynamics simulations. The colored points and vertical lines stand for the median value and the interquartile range (IQR) of each property measured, respectively. **** represent *p*-value adjusted (Bonferroni) = 0 on a Wilconsox Rank Sum test.

**Table 1. BS residues of K$_v$1.5 centroids.** Description of the binding site residues from centroid structures in K$_v$1.5 obtained by clustering based on physicochemical properties. For K$_v$1.5, centroid structures correspond to *K$_v$1.5_c1* and *K$_v$1.5_c2* from clusters 1 and 2, respectively.

| Unique *K$_v$1.5_c1* Residue | Common Residues | Unique *K$_v$1.5_c2* Residues |
|---|---|---|
| PRO513.B | MET478.A | GLY504.A |
| VAL516.B | THR479.A | VAL505.A |
| LEU506.C | THR480.A | ALA509.A |
| ALA509.C | VAL481.A | LEU437.B |
| VAL512.C | ILE508.A | LEU441.B |
|  | MET478.B | ALA501.C |
|  | THR479.B | ILE502.C |
|  | THR480.B | VAL512.D |
|  | ALA501.B |  |
|  | ILE502.B |  |
|  | GLY504.B |  |
|  | VAL505.B |  |
|  | ILE508.B |  |
|  | ALA509.B |  |
|  | VAL512.B |  |
|  | VAL505.C |  |

**Table 2. BS residues of Na$_v$1.5 centroids.** Description of the binding site residues from centroid structures in Na$_v$1.5 obtained by clustering based on physicochemical properties. For Na$_v$1.5, centroid structures correspond to *Na$_v$1.5_c1* and *Na$_v$1.5_c2* from clusters 1 and 2, respectively.

| Unique *Na$_v$1.5_c1* Residues | Common Residues | Unique *Na$_v$1.5_c2* Residues |
|---|---|---|
| TRP375.DI | THR371.DI | LEU410A.DI |
| PHE403.DI | GLN372.DI | LEU936.DII |
| SER402.DI | VAL406.DI | MET370.DI |
| ALA1418.DIII | LEU847.DII | PHE895.DII |
| LYS1421.DIII | LEU898.DII | PHE937.DII |
| THR1711.DIV | CYS899.DII | |
| ALA1713.DIV | GLY900.DII | |
| | MET926.DII | |
| | ASN930.DII | |
| | VAL933.DII | |
| | LEU934.DII | |
| | THR1419.DIII | |
| | PHE1420.DIII | |
| | ILE1456.DIII | |
| | ILE1457.DIII | |
| | PHE1461.DIII | |
| | LEU1464.DIII | |
| | SER1712.DIV | |
| | PHE1762.DIV | |
| | VAL1765.DIV | |

**Table 3. Comparison of binding sites from centroids using PocketMatch and their corresponding values of similarity score (%).** For K$_v$1.5, centroid structures correspond to *K$_v$1.5_c1* and *K$_v$1.5_c2* from clusters 1 and 2, respectively. In the case of Na$_v$1.5, *Na$_v$1.5_c1* and *Na$_v$1.5_c2* correspond to the two centroids from respective clusters 1 and 2.

| Centroid A | Centroid B | Similarity Score (%) |
|---|---|---|
| *K$_v$1.5_c2* | *K$_v$1.5_c1* | 95.2075 |
| *K$_v$1.5_c2* | *Na$_v$1.5_c1* | 72.2969 |
| ***K$_v$1.5_c2*** | ***Na$_v$1.5_c2*** | **78.6090** |
| *K$_v$1.5_c1* | *Na$_v$1.5_c1* | 60.6061 |
| *K$_v$1.5_c1* | *Na$_v$1.5_c2* | 65.1748 |
| *Na$_v$1.5_c1* | *Na$_v$1.5_c2* | 83.2655 |

The *K$_v$1.5_c2* and *Na$_v$1.5_c2* centroids were used to explore the hypothesis of a common structural pattern in flecainide BS between K$_v$1.5 and Na$_v$1.5 channels. BSs from *K$_v$1.5_c2* and *Na$_v$1.5_c2* structures were aligned using PocketAlign. As a result, a pairwise list of equivalent residues was obtained and, then, filtered using as cutoff a contact frequency equal to or greater than 70%. The amino acids resulting from PocketAlign analysis were distinguished by their physicochemical nature following PocketMatch classification. Ten residue equivalence was retrieved using PocketAlign (Figure 6 and Table 4). Residue equivalence numbers from 1 to 6 exhibit a similar physicochemical nature. Four of them (1, 2, 3 and 4) correspond to aliphatic, non-polar and uncharged amino acids (Figure 6a,b and Table 4). The other two (5 and 6) correspond to aliphatic, polar amino acids with hydroxy or mercapto groups. Equivalences from 7 to 10 do not share similar physicochemical features. Note that residue equivalence from 1 to 8 is well-fitted in the structural alignment (Figure 6c).
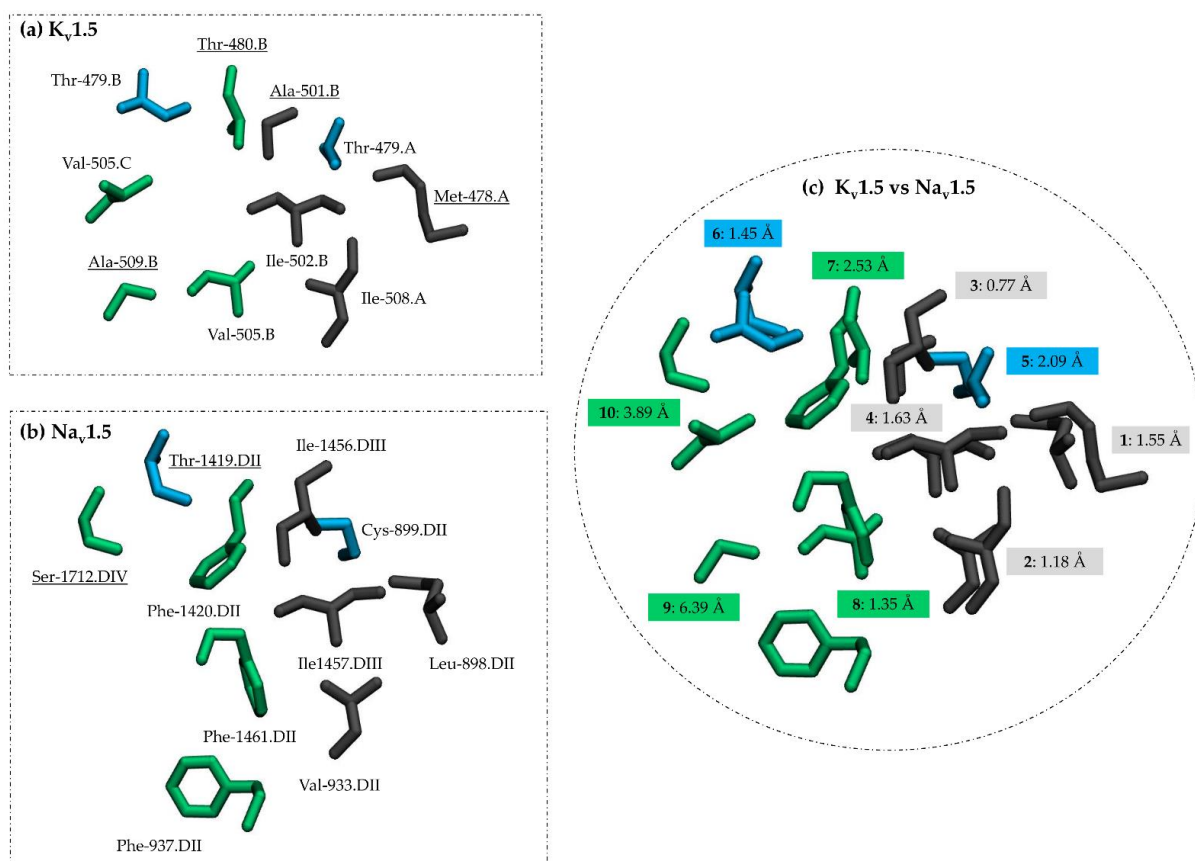
**Figure 6. Structural alignment of equivalent residues in flecainide BS.** The equivalent residues of flecainide BS in (**a**) $K_v1.5$, (**b**) $Na_v1.5$ and (**c**) their superposition according to PocketAlign comparison are displayed. Only residues with a contact frequency ≥70% are shown. In (**c**), the equivalences are numbered from 1 to 10 similar to Table 4. The underlined residues were not previously reported in flecainide BS. In addition, the distances between the centers of mass of the equivalent residues are appended.

**Table 4. List of equivalent residues in $K_v1.5$ and $Na_v1.5$ flecainide BS according to PocketAlign predictions.** The structures used for comparison correspond to centroids *$K_v1.5\_c2$* and *$Na_v1.5\_c2$*. Only the residues with a frequency of contact ≥70% are considered. The asterisk indicates residues relevant for flecainide bindings as reported by mutagenesis in $K_v1.5$ and cryo-EM $Na_v1.5$-flecainide structure [20,21]. Residues were classified according to their PocketMatch physicochemical nature description in (**a**) aliphatic, non-polar and uncharged; (**b**) aliphatic, polar with hydroxy or mercapto group; (**c**) aromatic, uncharged amino acid. Type of interaction information comes from Figures 2b and 4b for $K_v1.5$ and $Na_v1.5$, respectively.

| No. | *$K_v1.5\_c2$* | Physicochemical Nature/Int | *$Na_v1.5\_c2$* | Physicochemical Nature/Int |
|---|---|---|---|---|
| 1 | MET478A | a | LEU898.DII * | a/halogen bonds |
| 2 | ILE508A * | a/hydrophobic int. | VAL933.DII * | a/hydrophobic int. |
| 3 | ALA501B | a | ILE1456.DIII * | a/halogen bonds |
| 4 | ILE502B * | a | ILE1457.DIII * | a |
| 5 | THR479A * | b/halogen bonds | CYS899.DII * | b/halogen bonds |
| 6 | THR479B * | b/halogen bonds | THR1419.DII | b/water bridges |
| 7 | THR480B | b/hydrophobic int., water bridges | PHE1420.DII * | c/hydrophobic int., π stacks |
| 8 | VAL505B * | a/hydrophobic int. | PHE1461.DII * | c/hydrophobic int., π stacks |
| 9 | ALA509B | a/hydrophobic int. | PHE937.DII * | c/hydrophobic int., π stacks |
| 10 | VAL505C * | a | SER1712.DIV | b/water bridges |

Int: interaction, No.: number of residue equivalence.

The matching residues, represented with surfaces in Figure 7, occupy the central cavity in both channels, the B-C subunit interface in $K_v1.5$ and fenestration DII-DIII in $Na_v1.5$. Figure 7 shows the common structural pattern. Equivalent residues from 1 to 6 form two elements in the flecainide BS: (1) a hydrophobic patch (Figure 7, see residue surface in color gray) comprised of residues Met-478.A, Ile-508.A, Ala-501.B, Ile-502.B in $K_v1.5$ (Figure 7a) and Leu-898.DII, Val-933.DII, Ile-1456.DIII, Ile-1457.DIII in $Na_v1.5$ (Figure 7b) and (2) a polar region (Figure 7, see residue surface in color blue) comprising Thr-479.A and Thr-479.B in $K_v1.5$ (*zoom* in Figure 7a) and Cys-899.DII and Thr-1419.DIII in $Na_v1.5$ (Figure 7b).
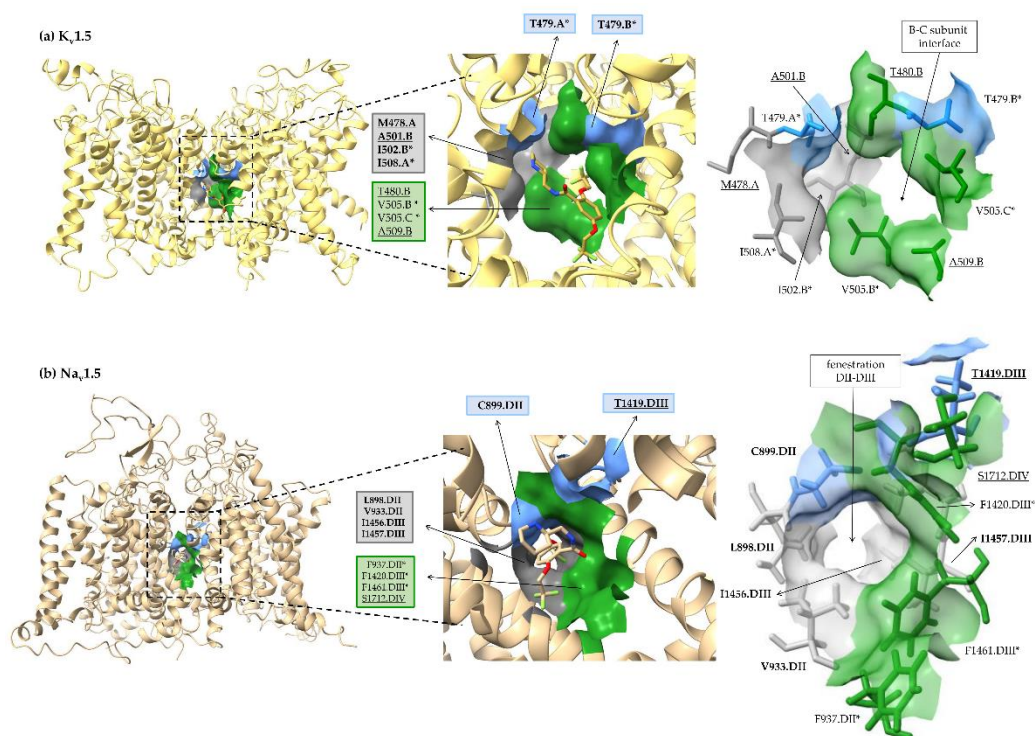


**Figure 7. Mapping onto tertiary structure the equivalent residues in flecainide BS**. Surface representation of the equivalent residues in flecainide BS in (**a**) $K_v1.5$ and (**b**) $Na_v1.5$ as predicted by PocketAlign (listed in Table 4). Residues from the hydrophobic patch are shown in gray surface and they are labeled inside a gray box meanwhile those from the hydrophilic region are highlighted in light-blue and included in a box with similar color. The rest of equivalent residues are presented in green surface and they are enclosed in a green box. The equivalent residues with a similar physicochemical nature are highlighted in bold.——The * is used to denote residues relevant for flecainide binding according to mutagenesis in $K_v1.5$ and cryo-EM flecainide-bound structure in $Na_v1.5$. The underlined residues were not previously reported in flecainide BS. Flecainide is shown in sticks and colored *per* element with oxygen atoms in red, nitrogen atoms in blue, fluorine atoms in green and carbon atoms in sand color.

## 4. Discussion

When comparing flecainide poses in $Na_v1.5$ and $K_v1.5$ channels, we detected a consensus binding mode where the drug fits the central cavity with extensions to the lateral sides of the channel (Figures 1a and 3a). In particular, the flecainide piperidine ring faces the inner cavity at the base of the SF; the aromatic moiety fits in the hydrophobic environment in the low levels of the inner cavity; and the trifluoromethyl moieties protrude to lateral sides (fenestration DII-DIII in $Na_v1.5$ and subunit interface B-C in $K_v1.5$). This binding mode resembles an angular conformation already predicted for long and flexible ligands in $K_v1.5$ [59].

The protonated piperidine moiety sits in the cation attractive region close to the base of the SF [60] in both channels (Figures 1a and 3a). In previous reports, the cationic groups of charged ligands bound to voltage-gated sodium and potassium channels are also attracted to the SF and occupy sites for permanent sodium ions in Nav channels [60]. In $Na_v1.5$, the charged ammonium group exerts a pivotal role in flecainide-associated inhibition [57]. The sodium channel blocked by flecainide and two derivatives (one neutral and the other fully charged at a physiological pH) disclose that the blockade results from the interaction of the cationic form [57].

The comparative analysis of flecainide BS in $K_v1.5$ and $Na_v1.5$ highlighted that the presence of aromatic residues is a key distinguished feature in $Na_v1.5$ (Figures 1b and 3b). Importantly, three aromatic residues—Phe-937.DII, Phe-1420.DIII and Phe-1461.DIII—in $Na_v1.5$ have π-stacking interactions with the phenyl ring of flecainide, and Phe-1762.DIV exhibits hydrophobic interactions with the piperidine moiety (Figures 3b and 4b). Phe-1760 in $hNa_v1.5$ (homolog to Phe-1762 in $rNa_v1.5$) plays a role in local anesthetics and antiarrhythmic action [49,50]. In our predictions, the residue Phe-1762.DIV is close to the positively charged piperidine ring but establishes only hydrophobic interactions (Figure 4b). This residue usually establishes a cation-π interaction with charged drugs with some exceptions, including flecainide and ranolazine [61,62]. Our results are in agreement with experimental evidence probing that flecainide does not require the cation-π interaction with Phe-1760 for its binding and use-dependent blockade [62].

Previously, the influence of aromatic residues in the $K_v1.5$ inner cavity was addressed by mutagenesis studies [21]. The substitutions of I502F and I508F in $hK_v1.5$ increase the $IC_{50}$ (164.49 μM ± 31.36 and 74.71 μM ± 5.37, respectively) compared to the wild-type ($IC_{50}$ = 38.14 μM ± 1.06) [21]. Then, aromatic moieties disturb drug interactions in such positions. However, a similar mutation at position 505 (V505F) increases flecainide affinity for $hK_v1.5$; the $IC_{50}$ value decreases to 4.27 μM in HEK 293 cells [21]. A possible explanation was given by Eldstrom et al., 2007 [21]. They presume that substitution V505F could favor cation-π interactions with piperidine from flecainide. However, using our model, we suggest that the substitution of V505F could favor π-stacking interactions with the phenyl aromatic ring of flecainide. As shown in Figure 1b, the residue Val-505.C is placed in front of the phenyl ring of flecainide. Then, the localization of an aromatic residue close to the flecainide phenyl ring is likely to account for a higher affinity binding.

Considering all the previous discussion, we proposed that aromatic moieties (Phe-937.DII, Phe-1420.DIII and Phe-1461.DIII and Phe-1762.DIV) in $Na_v1.5$ could explain flecainide's higher affinity for this channel than $K_v1.5$. Phe-1762.DIV is located in front of the flecainide piperidine ring but only establishes hydrophobic interactions (Figures 3b and 4b). Residue Phe-1420.DIII and, to a minor extent, Phe-1461.DIII and Phe-937.DII are all placed near the flecainide phenyl ring (Figure 3b) [20]. Phe-1762.DIV has been extensively studied and recognized as a relevant interacting residue for local anesthetics and antiarrhythmics binding [49,50]. However, to the best of our knowledge the possible contribution of Phe-937.DII, Phe-1420.DIII and Phe-1461.DIII for high-affinity ligand binding in $Na_v1.5$ is still not reported.

Our hypothesis for high-affinity flecainide binding in $Na_v1.5$ is consistent with previous studies in potassium channel hERG, another high-affinity target of flecainide [25]. Melgari et al. revealed the importance of the aromatic residue Phe-656 as a principal binding determinant for flecainide. These authors found that mutant F656A in hERG increased he t$IC_{50}$ 142-fold compared to the wild-type [25]. They argued that Phe-656 (from two different chains) interacts with two different moieties in the flecainide molecule. In detail, Phe-656 interacts with the benzamide moiety and the piperidine ring of flecainide [25]. We speculate that Phe-656 in hERG plays a similar role to Phe-1762.DIV in $Na_v1.5$. In hERG and $Na_v1.5$, respective aromatic residues Phe-656 and Phe-1762.DI are placed in front of the piperidine ring, respectively [20,21]. Interestingly, Phe-656 does not have a homolog aromatic residue counterpart in $K_v1.5$, since, according to sequence alignments, Phe-656 corresponds to Val-512 in $K_v1.5$ [63]. Our findings and those published by Melgari et al. [25] support the

need for aromatic residues for high-affinity binding of flecainide in their preferred targets, $Na_v1.5$ and hERG. Accordingly, we propose that the absence of aromatic residues in $K_v1.5$ could explain the lower affinity for flecainide.

Although there was a distinctive presence of aromatic residues in $Na_v1.5$, we found the flecainide BS shares similarities in both channels (Table 3). In detail, we identified similar geometrical and physiochemical properties. Both flecainide pockets are hydrophobic, although $K_v1.5$ to a lesser extent (Figure 5c,e). This is a typical feature of multi-target drug BSs [64]. In agreement with previous observation, we revealed that most equivalent residues in flecainide BSs have a hydrophobic nature (Table 4 and Figure 6a,b).

As reported in Ehrt et al., the geometrical feature seems to be the most relevant determinant for promiscuous BS, increasing the chance of MTDL behavior [64]. As already mentioned, our comparative analysis of flecainide BSs revealed a similar geometry. The latter is denoted by the structurally equivalent residue pairs listed in Table 4 and shown in Figure 6. For most of them, the distance between their center of mass is lower than 2.5 Å (Figure 6c). The matching residues, represented with surfaces in Figure 7, occupy the central cavity in both channels, the B-C subunit interface in $K_v1.5$ and fenestration DII-DIII in $Na_v1.5$.

At the end of our computational workflow, we were able to identify a common structural pattern at flecainide BSs in $Na_v1.5$ and $K_v1.5$ channels (Scheme 1). Equivalent residues from 1 to 6 form two common elements in the flecainide BS: (1) a hydrophobic patch (see residue surface in color gray, Figure 7) comprised by residues Met-478.A, Ile-508.A, Ala-501.B, Ile-502.B in $K_v1.5$ (Figure 7a) and Leu-898.DII, Val-933.DII, Ile-1456.DIII, Ile-1457.DIII in $Na_v1.5$ (Figure 7b), and (2) a polar region (Figure 7, see residue surface in color blue) comprising Thr-479.A and Thr-479.B in $K_v1.5$ (Figure 7a) and Cys-899.DII and Thr-1419.DIII in $Na_v1.5$ (Figure 7b). These two regions could be hot spots for a drug-protein interaction in atrial-selective MTDL design strategies for AF.

The residue Ile-508.A (included in the groups of aliphatic, non-polar or uncharged amino acids) (Table 4) exhibits a hydrophobic interaction along MD simulation (Figure 2b). Likewise, Val-933.DII (equivalent to Ile-508.A) in $Na_v1.5$ presents a hydrophobic interaction with flecainide (Figure 4b). Regarding amino acid pairs that contain aliphatic, polar amino acids or a hydroxy or mercapto group, residue Thr-479.A exhibits halogen bonds' interaction in $K_v1.5$ (Figure 2b). Similar, its corresponding residue Cys-899.DII in $Na_v1.5$ displays halogen bonds (Figure 4b). Four pairs of equivalent residues differ in their physicochemical nature according to PocketMatch classification (Table 4, numbers 7 to 10), but three of them establish similar interactions with flecainide. The $K_v1.5$ residue Thr-480.B presents the hydrophobic interaction as well as its pair Phe-1420.DIII in $Na_v1.5$. Val-505.B and Phe-1461.DIII display both hydrophobic interactions. Ala-509.B from $K_v1.5$ and Phe-937.DII in $Na_v1.5$ also present hydrophobic interactions with flecainide. Among these equivalent residue pairs, all the Phe from $Na_v1.5$ are highlighted as part of the flecainide BS in the cryo-EM holo structure (PDB code: 6UZ3) [20]. These Phe have distinctive π-stacking interactions from $K_v1.5$. Mainly, Phe-1420.DIII has the greatest π-stacking interaction. Some of the equivalent residue pairs, Thr-479, Ile-502, Val-505 and Ile-508, have recognized roles in flecainide binding in $K_v1.5$ as determined by mutagenesis [21].

As discussed above, the flecainide interaction profile (with the equivalent residues) differs in $K_v1.5$ and $Na_v1.5$ by about 50% (only five from ten residues exhibit similar interactions). However, this usually occurs for promiscuous drugs where the protein-ligand interaction profiles are not well related [64]. We found interactions that have relatively frequent (π stacking) or rare (halogen bond) prevalence in the PDB database [65] in $K_v1.5$ and $Na_v1.5$ flecainide BSs. Water bridges could contribute to flecainide binding because of their relevant role in ligand affinity and selectivity [66].

## 5. Conclusions

Besides flecainide, most ADDs are promiscuous in their action mechanism, and little is known about the structural basis of such behavior. One possible explanation is that they can

modify membrane properties [67]. However, the existence of ion channels' structure in the complex with ligands in combination with mutagenesis studies reporting the binding site of antiarrhythmics suggests that direct binding is also playing a role in promiscuity activity, and it is likely that common structural similarities are present at the antiarrhythmic BSs.

In the context of AF, mathematical models revealed that a promiscuity drug action focused on atrial-selective targets could be a safer and more efficacious alternative approach to treat this disease [14,15]. We focused on atrial-selective targets $K_v1.5$ and $Na_v1.5$ and their common blocker flecainide; we performed a comparative study of BSs for this drug coupling docking, MD and pocket comparison.

Our study identified that $K_v1.5$ and $Na_v1.5$ shared several common residues required for flecainide binding. The majority of these counterpart residues have similar geometrical and physiochemical properties. This led us to propose a common structural pattern for flecainide BS. Such a common pattern consists of two matching areas: a hydrophobic patch and a polar region. We also found a distinctive feature only present in $Na_v1.5$, which could be responsible for flecainide's higher affinity in $Na_v1.5$ versus $K_v1.5$, which is the presence of aromatic residues and their associated putative $\pi$-stacking interactions. Another critical aromatic residue in $Na_v1.5$ for local anesthetic and AAD binding is Phe-1762 (Phe-1760 in humans). This residue does not exhibit an aromatic counterpart in $K_v1.5$. We speculate that Phe-1762 could also account for flecainide's high-affinity binding in $Na_v1.5$.

Our results are intended to be used in rational MTDL design and new discovery protocols. We propose that ligands in close contact with residues of the promiscuous BS found in $Na_V1.5$ and $K_v1.5$ channels would simultaneously exert a biological action in both channels. The protocol described here for the BS comparison could be extended to other systems, gaining knowledge of the structural basis of polypharmacological drugs' effects.

**Supplementary Materials:** The following supporting information can be downloaded at: https://www.mdpi.com/article/10.3390/pharmaceutics14071356/s1, Figure S1. Root-mean square deviation (RMSD) of proteins atoms. The RMSD average value (colored points) from the three molecular dynamics (MD) replicas of $K_v1.5$ and $Na_v1.5$ apo and holo systems (flecainide-bound) are displayed. Verticals lines represent the RMSD standard deviation. RMSD were computed regarding the first frame of each MD. SD: standard deviation; Figure S2. The Root Mean Square Fluctuation (RMSF) of residue atoms. Average of RMSF (colored points) from the three MD replicas, comparing with the first frame, are shown in apo and holo systems. Verticals lines represent the RMSF standard deviation. The residues relevant for flecainide bindings as reported by mutagenesis in $K_v1.5$ and cryo-EM $Na_v1.5$-flecainide structure are indicated [20,21]. (a) For $K_v1.5$, the regions corresponding to transmembrane segments S1-S6 for each A, B, C and D subunits are indicated. Missing RMSF values corresponds to gap regions in $K_v1.5$ model (residues from loop S1–S2 and loop S3–S4) (b) For $Na_v1.5$, domains DI–DIV are labeled. The gap corresponds to the missing residues from linkers between domains DI–DII and DII–DIII; Figure S3. Radius profile of ion channel pore. The average radius value (colored point) from the three MDs replicas along z-axis. is displayed for (a) $K_v1.5$ and (b) $Na_v1.5$ in apo and holo systems. Horizontal lines represent the radius standard deviation. Black and red lines stand for selectivity filter and central cavity, respectively.

**Author Contributions:** Conceptualization, Y.M. and J.C.E.M.M.; methodology, Y.M. and J.C.E.M.M.; software, J.C.E.M.M.; validation, Y.M., J.C.E.M.M. and W.G.; formal analysis, Y.M., J.C.E.M.M. and W.G.; investigation, Y.M. and J.C.E.M.M.; resources, W.G.; data curation, J.C.E.M.M.; writing—original draft preparation, Y.M. and J.C.E.M.M.; writing—review and editing, W.G., D.R., L.Z., N.D., U.R. and V.Y.-Y.; visualization, Y.M. and J.C.E.M.M.; supervision, W.G.; project administration, W.G.; funding acquisition, W.G. All authors have read and agreed to the published version of the manuscript.

**Institutional Review Board Statement:** Not applicable.

**Informed Consent Statement:** Not applicable.

**Conflicts of Interest:** The authors declare no conflict of interest. The funders had no role in the design of the study; in the collection, analyses or interpretation of data; in the writing of the manuscript; or in the decision to publish the results.

# References

1. Chugh, S.S.; Havmoeller, R.; Narayanan, K.; Singh, D.; Rienstra, M.; Benjamin, E.J.; Gillum, R.F.; Kim, Y.-H.; McAnulty, J.H.; Zheng, Z.-J.; et al. Worldwide Epidemiology of Atrial Fibrillation: A Global Burden of Disease 2010 Study. *Circulation* **2014**, *129*, 837–847. [CrossRef]
2. Geng, M.; Lin, A.; Nguyen, T.P. Revisiting Antiarrhythmic Drug Therapy for Atrial Fibrillation: Reviewing Lessons Learned and Redefining Therapeutic Paradigms. *Front. Pharmacol.* **2020**, *11*, 581837. [CrossRef] [PubMed]
3. Peyronnet, R.; Ravens, U. Atria-Selective Antiarrhythmic Drugs in Need of Alliance Partners. *Pharmacol. Res.* **2019**, *145*, 104262. [CrossRef] [PubMed]
4. Ravens, U.; Poulet, C.; Wettwer, E.; Knaut, M. Atrial Selectivity of Antiarrhythmic Drugs. *J. Physiol.* **2013**, *591*, 4087–4097. [CrossRef] [PubMed]
5. Antzelevitch, C.; Burashnikov, A. Atrial-Selective Sodium Channel Block as a Novel Strategy for the Management of Atrial Fibrillation. *J. Electrocardiol.* **2009**, *42*, 543–548. [CrossRef] [PubMed]
6. Ravens, U. Atrial-Selective K$^+$ Channel Blockers: Potential Antiarrhythmic Drugs in Atrial Fibrillation? *Can. J. Physiol. Pharmacol.* **2017**, *95*, 1313–1318. [CrossRef]
7. Burashnikov, A.; Di Diego, J.M.; Zygmunt, A.C.; Belardinelli, L.; Antzelevitch, C. Atrial-Selective Sodium Channel Block as a Strategy for Suppression of Atrial Fibrillation. *Ann. N. Y. Acad. Sci.* **2008**, *1123*, 105–112. [CrossRef]
8. Ford, J.W.; Milnes, J.T. New Drugs Targeting the Cardiac Ultra-Rapid Delayed-Rectifier Current (I Kur): Rationale, Pharmacology and Evidence for Potential Therapeutic Value. *J. Cardiovasc. Pharmacol.* **2008**, *52*, 105–120. [CrossRef]
9. Ford, J.; Milnes, J.; Wettwer, E.; Christ, T.; Rogers, M.; Sutton, K.; Madge, D.; Virag, L.; Jost, N.; Horvath, Z.; et al. Human Electrophysiological and Pharmacological Properties of XEN-D0101: A Novel Atrial-Selective Kv1.5/IKur Inhibitor. *J. Cardiovasc. Pharmacol.* **2013**, *61*, 408–415. [CrossRef]
10. Pavri, B.B.; Greenberg, H.E.; Kraft, W.K.; Lazarus, N.; Lynch, J.J.; Salata, J.J.; Bilodeau, M.T.; Regan, C.P.; Stump, G.; Fan, L.; et al. MK-0448, a Specific Kv1.5 Inhibitor: Safety, Pharmacokinetics, and Pharmacodynamic Electrophysiology in Experimental Animal Models and Humans. *Circ. Arrhythm. Electrophysiol.* **2012**, *5*, 1193–1201. [CrossRef]
11. Van Wagoner, D.R. Multi-Channel Blockers for Treatment of Atrial Fibrillation: An Effective Strategy? *Cardiovasc. Res.* **2013**, *98*, 5–6. [CrossRef] [PubMed]
12. Reiffel, J.A.; Camm, A.J.; Belardinelli, L.; Zeng, D.; Karwatowska-Prokopczuk, E.; Olmsted, A.; Zareba, W.; Rosero, S.; Kowey, P. HARMONY Investigators The HARMONY Trial: Combined Ranolazine and Dronedarone in the Management of Paroxysmal Atrial Fibrillation: Mechanistic and Therapeutic Synergism. *Circ. Arrhythm. Electrophysiol.* **2015**, *8*, 1048–1056. [CrossRef]
13. Koskinas, K.C.; Fragakis, N.; Katritsis, D.; Skeberis, V.; Vassilikos, V. Ranolazine Enhances the Efficacy of Amiodarone for Conversion of Recent-Onset Atrial Fibrillation. *Europace* **2014**, *16*, 973–979. [CrossRef] [PubMed]
14. Aguilar, M.; Xiong, F.; Qi, X.Y.; Comtois, P.; Nattel, S. Potassium Channel Blockade Enhances Atrial Fibrillation-Selective Antiarrhythmic Effects of Optimized State-Dependent Sodium Channel Blockade. *Circulation* **2015**, *132*, 2203–2211. [CrossRef] [PubMed]
15. Ni, H.; Whittaker, D.G.; Wang, W.; Giles, W.R.; Narayan, S.M.; Zhang, H. Synergistic Anti-Arrhythmic Effects in Human Atria with Combined Use of Sodium Blockers and Acacetin. *Front. Physiol.* **2017**, *8*, 946. [CrossRef]
16. Jæger, K.H.; Edwards, A.G.; Giles, W.R.; Tveito, A. A Computational Method for Identifying an Optimal Combination of Existing Drugs to Repair the Action Potentials of SQT1 Ventricular Myocytes. *PLoS Comput. Biol.* **2021**, *17*, e1009233. [CrossRef]
17. Haupt, V.J.; Daminelli, S.; Schroeder, M. Drug Promiscuity in PDB: Protein Binding Site Similarity Is Key. *PLOS ONE* **2013**, *8*, e65894. [CrossRef]
18. Valdés-Jiménez, A.; Jiménez-González, D.; Kiper, A.K.; Rinné, S.; Decher, N.; González, W.; Reyes-Parada, M.; Núñez-Vivanco, G. A New Strategy for Multitarget Drug Discovery/Repositioning through the Identification of Similar 3D Amino Acid Patterns Among Proteins Structures: The Case of Tafluprost and Its Effects on Cardiac Ion Channels. *Front. Pharmacol.* **2022**, *13*, 761. [CrossRef]
19. Naderi, M.; Lemoine, J.M.; Govindaraj, R.G.; Kana, O.Z.; Feinstein, W.P.; Brylinski, M. Binding Site Matching in Rational Drug Design: Algorithms and Applications. *Brief. Bioinform.* **2019**, *20*, 2167–2184. [CrossRef]
20. Jiang, D.; Shi, H.; Tonggu, L.; Gamal El-Din, T.M.; Lenaeus, M.J.; Zhao, Y.; Yoshioka, C.; Zheng, N.; Catterall, W.A. Structure of the Cardiac Sodium Channel. *Cell* **2020**, *180*, 122–134.e10. [CrossRef]
21. Eldstrom, J.; Wang, Z.; Xu, H.; Pourrier, M.; Ezrin, A.; Gibson, K.; Fedida, D. The Molecular Basis of High-Affinity Binding of the Antiarrhythmic Compound Vernakalant (RSD1235) to Kv1.5 Channels. *Mol. Pharmacol.* **2007**, *72*, 1522–1534. [CrossRef] [PubMed]
22. Aliot, E.; Capucci, A.; Crijns, H.J.; Goette, A.; Tamargo, J. Twenty-Five Years in the Making: Flecainide Is Safe and Effective for the Management of Atrial Fibrillation. *Europace* **2011**, *13*, 161–173. [CrossRef] [PubMed]
23. Echt, D.S.; Ruskin, J.N. Use of Flecainide for the Treatment of Atrial Fibrillation. *Am. J. Cardiol.* **2020**, *125*, 1123–1133. [CrossRef] [PubMed]

24. Muzzey, M.; Tellor, K.B.; Ramaswamy, K.; Schwarze, M.; Armbruster, A.L. Flecainide Is Well-Tolerated and Effective in Patient with Atrial Fibrillation at 12 Months: A Retrospective Study. *Ther. Adv. Cardiovasc. Dis.* **2020**, *14*, 1753944720926824. [CrossRef] [PubMed]

25. Melgari, D.; Zhang, Y.; El Harchi, A.; Dempsey, C.E.; Hancox, J.C. Molecular Basis of HERG Potassium Channel Blockade by the Class Ic Antiarrhythmic Flecainide. *J. Mol. Cell. Cardiol.* **2015**, *86*, 42–53. [CrossRef]

26. Paul, A.A.; Witchel, H.J.; Hancox, J.C. Inhibition of the Current of Heterologously Expressed HERG Potassium Channels by Flecainide and Comparison with Quinidine, Propafenone and Lignocaine. *Br. J. Pharmacol.* **2002**, *136*, 717–729. [CrossRef] [PubMed]

27. Grissmer, S.; Nguyen, A.N.; Aiyar, J.; Hanson, D.C.; Mather, R.J.; Gutman, G.A.; Karmilowicz, M.J.; Auperin, D.D.; Chandy, K.G. Pharmacological Characterization of Five Cloned Voltage-Gated K$^+$ Channels, Types Kv1.1, 1.2, 1.3, 1.5, and 3.1, Stably Expressed in Mammalian Cell Lines. *Mol. Pharmacol.* **1994**, *45*, 1227–1234.

28. Herrera, D.; Mamarbachi, A.; Simoes, M.; Parent, L.; Sauvé, R.; Wang, Z.; Nattel, S. A Single Residue in the S6 Transmembrane Domain Governs the Differential Flecainide Sensitivity of Voltage-Gated Potassium Channels. *Mol. Pharmacol.* **2005**, *68*, 305–316. [CrossRef]

29. Salvage, S.C.; Chandrasekharan, K.H.; Jeevaratnam, K.; Dulhunty, A.F.; Thompson, A.J.; Jackson, A.P.; Huang, C.L. Multiple Targets for Flecainide Action: Implications for Cardiac Arrhythmogenesis. *Br. J. Pharmacol.* **2018**, *175*, 1260–1278. [CrossRef]

30. Kaminski, G.A.; Friesner, R.A.; Tirado-Rives, J.; Jorgensen, W.L. Evaluation and Reparametrization of the OPLS-AA Force Field for Proteins via Comparison with Accurate Quantum Chemical Calculations on Peptides. *J. Phys. Chem. B* **2001**, *105*, 6474–6487. [CrossRef]

31. Banks, J.L.; Beard, H.S.; Cao, Y.; Cho, A.E.; Damm, W.; Farid, R.; Felts, A.K.; Halgren, T.A.; Mainz, D.T.; Maple, J.R.; et al. Integrated Modeling Program, Applied Chemical Theory (IMPACT). *J. Comput. Chem.* **2005**, *26*, 1752–1780. [CrossRef] [PubMed]

32. Shivakumar, D.; Williams, J.; Wu, Y.; Damm, W.; Shelley, J.; Sherman, W. Prediction of Absolute Solvation Free Energies Using Molecular Dynamics Free Energy Perturbation and the OPLS Force Field. *J. Chem. Theory Comput.* **2010**, *6*, 1509–1519. [CrossRef] [PubMed]

33. Friesner, R.A.; Banks, J.L.; Murphy, R.B.; Halgren, T.A.; Klicic, J.J.; Mainz, D.T.; Repasky, M.P.; Knoll, E.H.; Shelley, M.; Perry, J.K.; et al. Glide: A New Approach for Rapid, Accurate Docking and Scoring. 1. Method and Assessment of Docking Accuracy. *J. Med. Chem.* **2004**, *47*, 1739–1749. [CrossRef] [PubMed]

34. Friesner, R.A.; Murphy, R.B.; Repasky, M.P.; Frye, L.L.; Greenwood, J.R.; Halgren, T.A.; Sanschagrin, P.C.; Mainz, D.T. Extra Precision Glide: Docking and Scoring Incorporating a Model of Hydrophobic Enclosure for Protein−Ligand Complexes. *J. Med. Chem.* **2006**, *49*, 6177–6196. [CrossRef] [PubMed]

35. Madhavi Sastry, G.; Adzhigirey, M.; Day, T.; Annabhimoju, R.; Sherman, W. Protein and Ligand Preparation: Parameters, Protocols, and Influence on Virtual Screening Enrichments. *J. Comput. Aided Mol. Des.* **2013**, *27*, 221–234. [CrossRef]

36. Bowers, K.; Chow, E.; Xu, H.; Dror, R.O.; Eastwood, M.P. Scalable Algorithms for Molecular Dynamics Simulations on Commodity Clusters. In Proceedings of the 2006 ACM/IEEE Conference on Supercomputing, Tampa, FL, USA, 11–17 November 2006; Volume 6, pp. 7695–7700.

37. Marzian, S.; Stansfeld, P.J.; Rapedius, M.; Rinné, S.; Nematian-Ardestani, E.; Abbruzzese, J.L.; Steinmeyer, K.; Sansom, M.S.P.; Sanguinetti, M.C.; Baukrowitz, T.; et al. Side Pockets Provide the Basis for a New Mechanism of Kv Channel-Specific Inhibition. *Nat. Chem. Biol.* **2013**, *9*, 507–513. [CrossRef]

38. Cheng, A.; Merz, K.M. Application of the Nosé−Hoover Chain Algorithm to the Study of Protein Dynamics. *J. Phys. Chem.* **1996**, *100*, 1927–1937. [CrossRef]

39. Martyna, G.J.; Tobias, D.J.; Klein, M.L. Constant Pressure Molecular Dynamics Algorithms. *J. Chem. Phys.* **1994**, *101*, 4177–4189. [CrossRef]

40. Humphrey, W.; Dalke, A.; Schulten, K. VMD: Visual Molecular Dynamics. *J. Mol. Graph.* **1996**, *14*, 33–38. [CrossRef]

41. Smart, O.S.; Neduvelil, J.G.; Wang, X.; Wallace, B.A.; Sansom, M.S. HOLE: A Program for the Analysis of the Pore Dimensions of Ion Channel Structural Models. *J. Mol. Graph.* **1996**, *14*, 354–360. [CrossRef]

42. Fpocket: An Open Source Platform for Ligand Pocket Detection—PubMed. Available online: https://pubmed.ncbi.nlm.nih.gov/19486540/ (accessed on 17 June 2022).

43. Monera, O.D.; Sereda, T.J.; Zhou, N.E.; Kay, C.M.; Hodges, R.S. Relationship of Sidechain Hydrophobicity and Alpha-Helical Propensity on the Stability of the Single-Stranded Amphipathic Alpha-Helix. *J. Pept. Sci.* **1995**, *1*, 319–329. [CrossRef] [PubMed]

44. Salentin, S.; Schreiber, S.; Haupt, V.J.; Adasme, M.F.; Schroeder, M. PLIP: Fully Automated Protein-Ligand Interaction Profiler. *Nucleic Acids Res.* **2015**, *43*, W443–W447. [CrossRef] [PubMed]

45. Adasme, M.F.; Linnemann, K.L.; Bolz, S.N.; Kaiser, F.; Salentin, S.; Haupt, V.J.; Schroeder, M. PLIP 2021: Expanding the Scope of the Protein-Ligand Interaction Profiler to DNA and RNA. *Nucleic Acids Res.* **2021**, *49*, W530–W534. [CrossRef] [PubMed]

46. Charrad, M.; Ghazzali, N.; Boiteau, V.; Niknafs, A. NbClust: An R Package for Determining the Relevant Number of Clusters in a Data Set. *J. Stat. Softw.* **2014**, *61*, 1–36. [CrossRef]

47. Yeturu, K.; Chandra, N. PocketMatch: A New Algorithm to Compare Binding Sites in Protein Structures. *BMC Bioinform.* **2008**, *9*, 543. [CrossRef] [PubMed]

48. Yeturu, K.; Chandra, N. PocketAlign a Novel Algorithm for Aligning Binding Sites in Protein Structures. *J. Chem. Inf. Model.* **2011**, *51*, 1725–1736. [CrossRef]

49.	Ragsdale, D.S.; McPhee, J.C.; Scheuer, T.; Catterall, W.A. Common Molecular Determinants of Local Anesthetic, Antiarrhythmic, and Anticonvulsant Block of Voltage-Gated Na$^+$ Channels. *Proc. Natl. Acad. Sci. USA* **1996**, *93*, 9270–9275. [CrossRef]

50.	Ragsdale, D.S.; McPhee, J.C.; Scheuer, T.; Catterall, W.A. Molecular Determinants of State-Dependent Block of Na$^+$ Channels by Local Anesthetics. *Science* **1994**, *265*, 1724–1728. [CrossRef]

51.	Nguyen, P.T.; DeMarco, K.R.; Vorobyov, I.; Clancy, C.E.; Yarov-Yarovoy, V. Structural Basis for Antiarrhythmic Drug Interactions with the Human Cardiac Sodium Channel. *Proc. Natl. Acad. Sci. USA* **2019**, *116*, 2945–2954. [CrossRef]

52.	Kiper, A.K.; Bedoya, M.; Stalke, S.; Marzian, S.; Ramírez, D.; de la Cruz, A.; Peraza, D.A.; Vera-Zambrano, A.; Márquez Montesinos, J.C.E.; Arévalo Ramos, B.A.; et al. Identification of a Critical Binding Site for Local Anaesthetics in the Side Pockets of Kv 1 Channels. *Br. J. Pharmacol.* **2021**, *178*, 3034–3048. [CrossRef]

53.	Kiper, A.K.; Rinné, S.; Rolfes, C.; Ramírez, D.; Seebohm, G.; Netter, M.F.; González, W.; Decher, N. Kv1.5 Blockers Preferentially Inhibit TASK-1 Channels: TASK-1 as a Target against Atrial Fibrillation and Obstructive Sleep Apnea? *Pflugers Arch.* **2015**, *467*, 1081–1090. [CrossRef] [PubMed]

54.	Decher, N.; Pirard, B.; Bundis, F.; Peukert, S.; Baringhaus, K.-H.; Busch, A.E.; Steinmeyer, K.; Sanguinetti, M.C. Molecular Basis for Kv1.5 Channel Block: Conservation of Drug Binding Sites among Voltage-Gated K$^+$ Channels. *J. Biol. Chem.* **2004**, *279*, 394–400. [CrossRef] [PubMed]

55.	Heginbotham, L.; Lu, Z.; Abramson, T.; MacKinnon, R. Mutations in the K$^+$ Channel Signature Sequence. *Biophys. J.* **1994**, *66*, 1061–1067. [CrossRef]

56.	Yue, L.; Feng, J.L.; Wang, Z.; Nattel, S. Effects of Ambasilide, Quinidine, Flecainide and Verapamil on Ultra-Rapid Delayed Rectifier Potassium Currents in Canine Atrial Myocytes. *Cardiovasc. Res.* **2000**, *46*, 151–161. [CrossRef]

57.	Liu, H.; Atkins, J.; Kass, R.S. Common Molecular Determinants of Flecainide and Lidocaine Block of Heart Na$^+$ Channels: Evidence from Experiments with Neutral and Quaternary Flecainide Analogues. *J. Gen. Physiol.* **2003**, *121*, 199–214. [CrossRef] [PubMed]

58.	Clustering Molecular Dynamics Trajectories for Optimizing Docking Experiments. Available online: https://www.hindawi.com/journals/cin/2015/916240/ (accessed on 18 February 2022).

59.	Tikhonov, D.B.; Zhorov, B.S. Homology Modeling of Kv1.5 Channel Block by Cationic and Electroneutral Ligands. *Biochim. Biophys. Acta (BBA)-Biomembr.* **2014**, *1838*, 978–987. [CrossRef]

60.	Tikhonov, D.B.; Zhorov, B.S. Mechanism of Sodium Channel Block by Local Anesthetics, Antiarrhythmics, and Anticonvulsants. *J. Gen. Physiol.* **2017**, *149*, 465–481. [CrossRef]

61.	Ahern, C.A.; Eastwood, A.L.; Dougherty, D.A.; Horn, R. Electrostatic Contributions of Aromatic Residues in the Local Anesthetic Receptor of Voltage-Gated Sodium Channels. *Circ. Res.* **2008**, *102*, 86–94. [CrossRef]

62.	Pless, S.A.; Galpin, J.D.; Frankel, A.; Ahern, C.A. Molecular Basis for Class Ib Anti-Arrhythmic Inhibition of Cardiac Sodium Channels. *Nat. Commun.* **2011**, *2*, 351. [CrossRef]

63.	Blunck, R.; Batulan, Z. Mechanism of Electromechanical Coupling in Voltage-Gated Potassium Channels. *Front. Pharmacol.* **2012**, *3*, 166. [CrossRef]

64.	Ehrt, C.; Brinkjost, T.; Koch, O. Binding Site Characterization - Similarity, Promiscuity, and Druggability. *Medchemcomm* **2019**, *10*, 1145–1159. [CrossRef] [PubMed]

65.	Ferreira de Freitas, R.; Schapira, M. A Systematic Analysis of Atomic Protein-Ligand Interactions in the PDB. *Medchemcomm* **2017**, *8*, 1970–1981. [CrossRef]

66.	Darby, J.F.; Hopkins, A.P.; Shimizu, S.; Roberts, S.M.; Brannigan, J.A.; Turkenburg, J.P.; Thomas, G.H.; Hubbard, R.E.; Fischer, M. Water Networks Can Determine the Affinity of Ligand Binding to Proteins. *J. Am. Chem. Soc.* **2019**, *141*, 15818–15826. [CrossRef] [PubMed]

67.	Rusinova, R.; Koeppe, R.E.; Andersen, O.S. A General Mechanism for Drug Promiscuity: Studies with Amiodarone and Other Antiarrhythmics. *J. Gen. Physiol.* **2015**, *146*, 463–475. [CrossRef] [PubMed]